Intriguing sequence of GaFeO_{3} structures and electronic states to 70 GPa

R. Arielly, W. M. Xu, E. Greenberg, G. Kh. Rozenberg, M. P. Pasternak, G. Garbarino, S. Clark, and R. Jeanloz

Phys. Rev. B **84**, 094109 — Published 19 September 2011

DOI: 10.1103/PhysRevB.84.094109

The intriguing sequence of $GaFeO_3$ structures and electronic states to 70 GPa.

R. Arielly,[a] W. M. Xu,[a] E. Greenberg,[a] G. Kh. Rozenberg,[a] M. P. Pasternak,[a*] G. Garbarino,[b] S. Clark,[c] and R. Jeanloz [d]

[a] School of Physics and Astronomy, Tel Aviv University, 69978, Tel Aviv, Israel
[b] European Synchrotron Radiation Facility (ESRF), 6 rue Jules Horowitz, BP 220, F-38043 Grenoble Cedex, France
[c] Advanced Light Source, Lawrence Berkeley National Laboratory, Berkeley, California 94720, USA
[d] Department of Geology and Geophysics, University of California, Berkeley, California 94720

ABSTRACT

Structural studies of the ferrimagnetic (T_N=200 K) *Mott* insulator $GaFeO_3$ (SG $Pc2_1n$) to 70 GPa, complemented by ^{57}Fe Mössbauer spectroscopy and resistance (R) measurements at compression, decompression and recompression reveal a fascinating sequence of structures. Starting at ~ 25 GPa a new structure, an orthorhombic perovskite (SG *Pbnm*), is sluggishly formed followed by a volume $V(P)$ drop of 5.4%. The complete formation of the perovskite occurs at 42 GPa. In the 0 – 33 GPa range T_N reaches 300 K and *R(P)* decreases by one-order of magnitude. At 53 GPa an isostructural transition is detected, characterized by a discontinuous drop of *V(P)* by ~3%. Mössbauer spectra reveal a non-magnetic component coexisting with the magnetic one at ~ 60 GPa. Its abundance increases and above 77 GPa no sign of a magnetic hyperfine interaction is detected down to 5 K. Concurrently, one observes a continuous yet precipitous decrease in $R(P)$ taking place in the 53-68 GPa range, leading to an onset of the metallic state at P = 68 GPa. These electronic/magnetic features of the high pressure (HP) perovskite are consistent with a *Mott* transition.

With pressure decrease, below 50 GPa, the insulating perovskite is recovered, and at ~24 GPa a 1st-order structural transition takes place to a $LiNbO_3$-type structure with SG *R3c*. This structure remains stable down to ambient pressure and with recompression it is stable up to 50 GPa, afterwards it transforms back to the HP perovskite structure. It is noteworthy that this transition occurs at the same pressure, regardless of the preceding structures: *Pbnm* or *R3c*. The results are compared with hematite (Fe_2O_3, SG $R\bar{3}c$) and other ferric oxides. The mechanisms of the transitions are discussed.

PACS number(s): 61.50.Ks, 62.50.-p, 71.30.+h, 61.05.cp, 76.80.+y

I. INTRODUCTION

Properties of the ferric oxides ($M^{3+}Fe^{3+}O_3$) at high pressure (HP) have become a subject of several recent studies [1, 2]. What has triggered the interest on the HP properties of these antiferromagnetic *Mott* insulators was the discovery [3] of the electronic mechanism responsible for the unusual ~ 10% volume shrinkage observed in Fe_2O_3 (hematite) at ~50 GPa [4]. In that case [5], a pressure-induced progressive distortion of the corundum like hematite structure was observed, preceding the transition and signifying the increasing asymmetry of the FeO_6 octahedra, which culminated in a first-order structural phase transition from a corundum to a Rh_2O_3(II)-type structure. The structural transition coincides with an insulator-metal transition and the collapse of the magnetic state (correlation breakdown). The fact that the Fe-O bonding is largely affected by the correlation breakdown implies that charge-transfer gap closure is the mechanism responsible for metallization, concurring with the collapse of the magnetic moments.

Whereas the structural transition in hematite clearly coincides with a *Mott* transition (MT) this was not the case in other ferric-oxides such as $RFeO_3$ ($R \equiv$ Rare Earth) [1] orthorhombic perovskites, where close to 40-50 GPa a HS-LS spin crossover takes place ($S = 5/2 \rightarrow S = 1/2$) concurrent with an isostructural phase transition and discontinuous volume reduction. Up to 170 GPa no Fe^{3+} moment collapse has been observed though an insulator-metal (IM) transition occurs at the 110-130 GPa range. It is noteworthy, that in $RFeO_3$ orthoferrites a precipitous resistance decrease was observed within the HS-LS coexistence range, suggesting that the HS-LS crossover in the Fe sublattice approaches a gap closure and metallization transition [1]. Recent studies of $BiFeO_3$ [2] have shown an onset of a MT at ~ 50 GPa triggered, as proposed by the authors, by the HS-LS crossover, which drives the effective correlation Mott-Hubbard energy U below the threshold of the IM transition.

The purpose of this work was to further elucidate the nature of the pressure-induced electronic transitions taking place at very high pressures, e.g., spin-crossover or *Mott* transition, and study its role upon consequential structural transitions in ferric oxides. $GaFeO_3$ (GFO) with its similar Ga^{3+} and Fe^{3+} ionic radii (0.62 Å and 0.64 Å), makes it an ideal candidate for such studies, particularly with respect to $FeFeO_3$. The structure of GFO resulting from high temperature synthesis is orthorhombic (space group (SG) $Pc2_1n$), with two Fe and two Ga located in four different sub-lattices: Fe1, Fe2 and Ga2, all 6-fold coordinated octahedra (O_h symmetry), and Ga1 in a 4-fold coordinated tetrahedron (T_d symmetry) (see Fig. 1). Ideal stoichiometric GFO and without site disorder is an antiferromagnetic insulator with Neel temperature $T_N = 200$ K [6].

Here we report the results of high-pressure studies to 100 GPa in diamond anvils cells combining the methods of synchrotron powder X-ray diffraction (XRD), Mössbauer spectroscopy, and resistance studies $R(P,T)$, allowing us to follow the pressure evolutions of the GFO structure, the Fe^{3+} spin state, and the possible pressure-induced collapse of the Mott-Hubbard gap . As will be seen, a rich

sequence of structural/electronic transitions takes place both at compression, decompression and recompression.

II. EXPERIMENTAL

Samples of $GaFeO_3$ were prepared by solid-state reaction of gallic and ferric oxides. High-purity (99.999%) powders of Ga_2O_3 and 40% isotopically-enriched $^{57}Fe_2O_3$ were thoroughly mixed, ground, pelletized and heated to 1300°C in an ambient atmosphere for 24 hours. After cooling for another day to room temperature, the pellet was ground, mixed, pressed, heated, and cooled again under the same conditions. Its structure and purity were verified with XRD and Mössbauer spectroscopy (see Fig. 2). As can be seen $T_N \sim 200$ K, confirms the purity and stoichiometry of the sample [7]. The sample was placed inside cylindrical cavities of a Re gasket following indentation to 30-μm thickness. TAU miniature opposing-plate and piston-cylinder diamond anvil cells (DAC) were used to generate pressures up to 70 and 100 GPa, respectively [8,9]. The anvil culets ranged from 200 to 500 μm in diameter with sample cavities from 100 x 30 μm to 250 x 50 μm. Liquid Ar was loaded as a pressure medium for both Mössbauer spectroscopy and XRD studies.

Mössbauer spectra (MS) at each pressure were recorded using a 10 mCi ^{57}Co point-source in the 4 – 300 K temperature range. Spectra were fitted using least-squares methods from which MS parameters were deduced: specifically, the *relative abundance* of the components, the *hyperfine field* $H_{hf}(P)$, the *isomer shift* IS(P), the *quadrupole splitting* QS(P) and the *magnetic ordering temperature* $T_N(P)$.

It should be noted that the complete decomposition of the magnetic and paramagnetic sub-spectra of the four crystallographic sites of Fe could not be carried out due to the finite resolution of the ^{57}Fe Mössbauer spectroscopy governed by its line-width. However, taking into account the similarity in the crystallographic surroundings for more than 90% of the Iron [6], the spectra could be safely fitted using one component [10] with a relatively broad line-width.

XRD measurements were carried out at room temperature in angle-dispersive mode with wavelength of 0.3738 Å and 0.41336 Å at ESRF, Grenoble, at the ID27 beam line and at ALS, Berkeley, at beam line 12.2.2 respectively. Diffraction images were collected using image plates or CCD. The image data were integrated using the FIT2D program [11,12] and the resulting diffraction patterns were analyzed with the GSAS [13,14] program.

Ruby R_1-line fluorescence spectroscopy was used [15, 16, 17] as a manometer for the Mössbauer spectroscopy and $R(P)$ studies, Pt [18] pressure markers were used for the XRD measurements.

Four-probe DC electrical resistance measurements as a function of pressure and temperature were carried using a stainless-steel gasket coated with Al_2O_3 into which a sample cavity of ~100-μm diameter was hand-drilled. Six electrodes of 5 – 7-μm thick Pt-foils were employed. At each pressure,

the DAC was immersed inside a liquid N_2- filled Dewar for measurements over the 80 - 300 K range. Temperature was determined using a Si-diode thermometer, and resistance values were derived from the measured I-V curves. Typical errors associated with pressure and temperature were ± 1 GPa and ± 0.5 K, respectively.

Experiments were carried out in the following pressure cycles: 1 – XRD, ^{57}Fe Mössbauer spectroscopy, and $R(P,T)$ measurements were carried during **compression** to 98 GPa, 2 – XRD and ^{57}Fe Mössbauer spectroscopy at **decompression** to ambient pressure, and 3 – XRD at **recompression** to 53 GPa.

III. RESULTS

Typical examples of full-profile fitted XRD spectra of the three structures emerged from this experiment, at pressure values in which there is no phase coexistence, are shown in Fig. 3: *i*) the orthorhombic $Pc2_1n$ (Z=8) phase which persists from ambient pressure to ~40 GPa, *ii*) the orthorhombic perovskite (SG *Pbnm* Z=4) present above 25 GPa both at compression and decompression and *iii*) the $LiNbO_3$-type phase (SG *R3c* Z=6) which emerged during decompression at 24 GPa and persisted down to ambient pressure. During recompression the *R3c* phase persists up to ~50 GPa after which it transforms to the orthorhombic perovskite (*Pbnm*). In Fig. 4 we recap the Equation of State ($V(P)$) of the three pressure paths: compression (filled symbols), decompression (open symbols) and recompression (filled symbols).

A. Compression

1. The 0 → 50 GPa isotherm

(a) *Structural properties* (see Figs. 3 and 4). Up to 25 GPa the $Pc2_1n$ symmetry is dominant with gradual volume decrease from 312 Å^3 at ambient pressure to 273 Å^3 at 42 GPa. In this range the XRD data was successfully fitted by solely varying the three lattice parameters with atomic positions fixed to those at ambient pressure [19] resulting in $\chi^2 < 0.12$, $w_{Rp} < 1.5\%$ and $Rp < 1\%$. The refined structural parameters obtained from the GSAS software are shown in Table 1. The $P(V)$ data for the $Pc2_1n$ phase was fitted to the 2nd order Birch-Murnaghan (BM2) Equation of State (EOS) [20] up to 40 GPa while fixing the first derivative of the bulk modulus to $K'=4$. The unit cell volume as a function of pressure is shown in Fig. 4. The resulting ambient pressure unit-cell volume, and bulk modulus are $V_0 = 312.2(4)$ Å^3 and $K_0 = 230(4)$ GPa, respectively.

At ~ 25 GPa a new phase starts evolving at the expense of the $Pc2_1n$. It is identified as the orthorhombic perovskite with SG *Pbnm* (Fig. 1). This phase can also be characterized in an orthorhombic setting by the three lattice parameters *a*, *b*, and *c,* but with only 4 possible atomic

positions. Following the work of Marezio *et al*. [21] concerning the rare earth orthoferrites (SG *Pbnm*), the atomic positions have been extrapolated according to the cation size of Ga. The data was successfully fitted by solely varying the three lattice parameters, with atomic positions fixed to the values extrapolated for ambient pressure, resulting in χ^2 being less than 0.025, w_{Rp}< 0.6% and Rp < 0.4%. The refined structural parameters are shown in Table 1. The transition to the perovskite phase is accompanied by a discontinuous volume change of – 5.4% (Fig. 4). The dotted line is a fit using a Birch-Murnaghan EOS resulting in K_0 = 296(25) GPa, K_0' = 4 (fixed), and V_0 = 291.7 (2.4) Å$^{3.}$ Unlike the orthorhombic $Pc2_1n$ phase, there is only one cationic site for Fe (six-fold coordinated) and one for Ga (8-fold coordinated) (Fig. 2). The coordination increase in Ga from four and six to eight is a possible leading mechanism behind this phase transition and the significant discontinuous volume decrease. Above 42 GPa only the perovskite structure is observed.

(b) *Electronic and magnetic properties*. Consistent with the volume decrease, the magnetic exchange interactions and therefore the ordering temperature increases with pressure (Fig. 5), starting from 200 K at ambient pressure and reaching 300 K at ~ 33 GPa. At P > 33 GPa $T_N(P)$ increases beyond 300 K but could not be quantified due to high temperature experimental limitations of the present MS system. Typical spectra at 15 K ($T << T_N$) is shown in Fig. 6. Up to 56 GPa there are no discernible changes in the low temperature Mössbauer spectra in which the single component displays a magnetic splitting with H_{hf} = 48(3) T.

The relative volume ($\Delta V/V_0$) dependence of the IS is shown in Fig. 7. [22]. The slope d(IS)/$d\ln(V)$, an atomic-scale property, remains rather constant and monotonic within the $Pc2_1n$ region and up to $\Delta V/V_0$ =0.22 (~60 GPa) This is in spite of the transition to the perovskite structure starting around 0.11 (~ 25 GPa) with its discontinuous volume decrease of ~5%. The reason being that the IS is directly related to the *s*-electron density $\rho_s(0)$ at the Fe nucleus [23]. Thus, upon pressure increase the density at the Fe vicinity increases, as expected, but it is not affected by the volume decrease taking place due to the discontinuous increase in the Ga coordination number.

Within the 0 – 31 GPa range ($Pc2_1n$ region), the resistance $R(\Delta V/V)$ decreases by one-order of magnitude (see Fig. 8). At higher pressures, within the pure *Pbnm* region (42 - 53 GPa range and up to $\Delta V/V_0$ = 0.2), $R(P)$ variation is more gradual. However, as shown in the lower inset, in this pressure range there is a continuous flattening of the $R(T)$ curves with pressure increase due to a decrease in the activation energy as expected from band broadening [24].

2. The 50 → 68 GPa isotherm

(a) *Structural evolution*. At ~ 53 GPa we witness (Fig. 4) a discontinuous reduction in volume $\Delta V/V_0$ ~ 3%. This structural transition carries no change in SG, namely, an isostructural transition. The data

was successfully fitted by solely varying the three lattice parameters resulting in $\chi^2 < 0.055$, $w_{Rp}<$ 0.8% and Rp < 0.6%. The refined structural parameters are shown in Table 1. The high pressure (HP) perovskite phase coexists with the lower pressure (LP) perovskite in the 53 – 54 GPa range. The dash-dotted line is a fit using a Birch-Murnaghan equation of state with variables $K_0 = 383(48)$ GPa, $K_0' = 4$ (fixed), and $V_0 = 275(4)$ Å^3.

(b) *Electronic and magnetic properties.* The MS(P) clearly shows a sluggish onset of a non-magnetic, quadrupole-split component, at $P > 56$ GPa coexisting with the magnetic component (Fig. 6). Its abundance increases with P and beyond 65 GPa this component becomes dominant. To ensure the absence of magnetism at lower temperatures characterized by the magnetic hyperfine interaction, spectra at $P > 65$ GPa were also recorded at 5 K [25]. As can be seen, the spectrum at 77 GPa and 5 K, in spite of the bad statistic, still shows remnants of a magnetic interaction component, characterized by H_{hf} of ~45T. However, the spectrum at 85 GPa shows no indications of magnetic interactions. The significant changes are also seen in T_N (P) (Fig. 5). Above 33 GPa T_N (P) crosses 300 K and near 67 GPa while descending it crosses 300 K again, reaching $T_N \sim 5$ K at 77 GPa. The IS($\Delta V/V_0$) curve shows a discontinuous sharp decrease in the 0.225 – 0.24 range (62-77 GPa) (Fig. 7). The relative abundance of the nonmagnetic-metallic phase associated with the HP-perovskite structure and derived from the Mössbauer spectra [26] increase sharply around $\Delta V/V_0 = 0.22$ reaching 1 at ~0.24 (~80 GPa) (see Fig. 7). Concurrently, one observes (Fig. 8) a continuous yet precipitous decrease in $R(\Delta V/V_0$,300K) taking place in the 0.20 – 0.23 range (53-68 GPa), leading to the onset of the metallic state at $P \sim 68$ GPa evident by the partially positive dR/dT (lower inset).

B. Decompression

1. The 68 → 24 GPa isotherm (see Fig. 4)

With decompression the HP perovskite structure dominates down to 50 GPa. At ~ 50 GPa it undergoes a discontinuous increase in V, with no hysteresis, eventually recovering the original LP perovskite structure and volume (Fig. 4, open symbols) characterized by its larger Fe^{3+} - O bond lengths reflecting the recovery of the correlated state.

2. The 24 → 0 GPa isotherm (Fig. 4)

At 24 GPa a dramatic structural first-order transition takes place. Diffraction patterns of the new phase can be fitted well with three different structures: corundum-type trigonal $(\mathrm{SG}\ R\bar{3}c)$, ilmenite $FeTiO_3$-type $(\mathrm{SG}\ R\bar{3})$ or $LiNbO_3$ (LN)-type $(\mathrm{SG}\ R3c)$. Taking into account that the derived c/a ratio of 2.699 is more typical for a LN structure than for ilmenite, as well as the better quality of the

fit results assuming a LN-phase, we discarded the ilmenite-type option. Although *R3c* and $R\bar{3}c$ structures show very similar quality of the fit: typical $\chi^2 \sim 0.017$, wRp< 0.46% and Rp < 0.36% one must take into account that the corundum-type structure does not differentiate between Ga and Fe sites which will result in random positions of the Fe magnetic moments leading to a disorder in the magnetic sublattices. In that case the MS would have shown features typical of *sites distributions*, e.g., broad and asymmetric absorption lines, which is not the case (Fig. 6). These arguments definitely favor the assignment of the new structure as the hexagonal $LiNbO_3$-type phase (Fig. 1) [27]. This phase can be characterized in a hexagonal setting by two lattice parameters *a*, and *c*, and 3 possible atomic positions. The latter values were taken from the work of Boysen *et al.* [28] and further refined for the spectrum at 0.2 GPa. Using the obtained atomic positions the data was successfully fitted by solely varying the two lattice constants. The refined structural parameters are shown in Table 2. The transition to the LN structure is accompanied by a small discontinuous increase in V (Fig. 4). This structure persists down to ambient pressure; the original $Pc2_1n$ phase is not recovered.

C. Recompression

The 0 → 53 GPa isotherm (see Fig. 4 and Table 2)

With recompression to ~ 50 GPa the *R3c* phase is fully preserved. The dashed line is a fit to all of the *R3c* points using a Birch-Murnaghan equation of state with variables $K_0 = 223(9)$ GPa, $K_0' = 4$ (fixed), and $V_0 = 298.7(8)$ Å^3. The gradual shrinkage in volume especially around 24 GPa, is not energetically sufficient to recover the *Pbnm* perovskite state. The phase is stable up to ~ 50 GPa, yet again at 50 GPa, due to the Fe^{3+}-O bond length shrinkage, the $LiNbO_3$-type structure becomes unstable and is replaced by the sturdier HP perovskite structure.

IV. DISCUSSION

By examining the MS(P), IS($\Delta V/V_0$), and $R(\Delta V/V_0,T)$ data as shown in Figs. 6-8, one comes to the conclusion that the breakdown of the magnetic moment along with evidence of a metallic behavior coincides with the *Mott* transition leading to the breakdown of the strong *d-d* correlation and therefore to the insulator-metal transition. At the compression isotherm one notices the striking features of $R(\Delta V/V_0)$, $\rho_s(\Delta V/V_0)$, and the non magnetic relative abundance ($\Delta V/V_0$) (Figs. 7, 8) convincing experimental evidence of this unusual electronic transition, e.g., the MT in Fe^{3+}.

Close to the critical pressure, when the Hubbard gap is small enough, electrons can be excited into the conduction band. In that case, disordering of the moments due to their coupling with the

excited electrons should be observed [29]. Such or similar changes of the electronic properties of the insulating magnetic phase near to the MT will result in the weakening of the super-exchange interactions and consequently in the drop in T_N (Fig. 5). Ultimately $GaFeO_3$ becomes non-magnetic and metallic at $P > 77$ GPa. Preceding this state a region of paramagnetic/non-magnetic coexistence should exist, in which insulating clusters of Fe^{3+} moments (S=5/2) and conducting nonmagnetic clusters coexist, the latter becoming dominant at $P > 68$ GPa.

Thus, the onset of the MT may explain the observed alterations of the structural, electronic and magnetic properties at pressures above 53 GPa. However, in spite of the sharp first-order structural transition observed at P~53 GPa, changes in the electronic/magnetic properties measured with MS and R take place above 53 GPa and continue sluggishly up to ~ 80 GPa. A systematic reason could be the two different types of manometries: the use of a Pt marker from which the pressure is deduced from the well know Pt-EOS and the ruby method. Another systematic reason could be the different geometries of the signal collection methods: the pressure is usually measured in the center of the sample cavity. Also, in the synchrotron XRD measurements the signal derives from a small central part of the sample, whereas in Mössbauer studies the signal is collected from a much larger part of the sample (~2/3) resulting in possible pressure gradient effects which could be significant. In resistivity measurements the role of pressure gradients could be also substantial [30]. It is important to note that in the 50-53 GPa range the Mössbauer spectra do not reveal any evidence of a preceding electronic transition, such as a spin-crossover, which could account for the observed volume decrease.

It will be interesting to compare the present results with the other MFeO$_3$ oxides in which XRD, spectroscopy and/or resistance were concurrently applied. As mentioned earlier, the RFeO$_3$ orthoferrites are an exception in the sense that at high pressure they undergo spin crossover (S=5/2 → S=1/2) transition at the 35 - 50 GPa range but do not undergo a MT to at least 170 GPa [1]. In what follows we compare GaFeO$_3$ with hematite (FeFeO$_3$) [3] and CaFe$_2$O$_4$ [31]. A common feature of all those ferric oxides is the discontinuous volume contraction occurring at ~ 50 GPa, when the relative volume of the Fe-O$_6$ polyhedral V_{pol}/V_{0pol} reaches 0.84-0.85.

Hematite at ambient conditions crystallizes in a corundum structure ($R\bar{3}c$) with six-coordinated Fe^{3+}. $GaFeO_3$ on the other hand, when synthesized at ambient pressure, crystallizes in an orthorhombic structure with SG $Pc2_1n$. Unlike hematite $GaFeO_3$ has two six-coordinated Fe-sites, one six-coordinated Ga-site, and one four-coordinated Ga-site. It is not surprising that this partially low-coordination species will not withstand the high-density regime. And indeed, a first-order structural phase transition takes place at ~25 GPa (V/V_0 ~ 0.91) into a sturdier orthorhombic perovskite (*Pbnm*) with a single six-coordinated Fe-O and a single eight-coordinated Ga-O building blocks. The molar volume of the perovskite is reduced by ~5% and its bulk modulus increases by ~

30%. With further pressure increase a second, albeit isostructural phase transition takes place at ~53 GPa (V_{pol}/V_{0pol} ~0.85, see inset Fig. 4) with a discontinuous volume decrease of ~3%. This reversible transition is concomitant with the *Mott* electronic transition of Fe^{3+}, the same one observed in Fe_2O_3 [3], in which the high-spin is transformed to a non-magnetic state.

Contrary to hematite, following decompression to ambient pressure, the *R3c* structure becomes the stable one. The reason that upon decompression perovskites (Pv) transform to LN-type instead of the original $Pc2_1n$ is a close structural relation of the LN- and Pv-type structures [32, 33]. Both structures consist of corner-linked FeO_6 octahedra, but in the Pv-type structure the adjacent octahedral layers are less tilted relative to one another. Therefore, in contrast to the $Pc2_1n$ structure, the octahedral framework can readily transform between the two structures by rotating them as rigid units, without breaking any bonds. The V_0 of the *R3c* phase is ~ 5% smaller than that of the $Pc2_1n$ phase but its bulk modulus K_0 remains almost the same and is practically identical to that of hematite [4, 34, 35]. At recompression the first-order structural phase transition takes place again at P~50 GPa (V_{pol}/V_{0pol} ~0.85), exactly as in Fe_2O_3 (P~50 GPa, V_{pol}/V_{0pol} ~0.84) [4,5]. The relative volume reduction at this point remains ~3% whereas in Fe_2O_3 it is ~10%. However, taking into account the corroborating transformation from corundum to Rh_2O_3-II structure [36], the part of the volume reduction associated with the electronic transition in Fe_2O_3 is ~6%, scaling well with the Fe/formula number: 1 in $GaFeO_3$ and 2 in Fe_2O_3. The corresponding shrinkage of the polyhedral volume in both systems is ~6%.

HP-XRD studies in $CaFe_2O_4$ (SG *Pbnm*) also reveal an abrupt volume decrease at 50 GPa (V_{pol}/V_{0pol} ~0.84). Though no $R(P,T)$ measurements were carried out, magnetic collapse is clearly observed by M. Merlini *et al*. [30] by X-ray emission spectroscopy and is consistent with a MT. However, in the case of $CaFe_2O_4$ the corresponding abrupt polyhedral volume decrease is ~12%, doubled in comparison to GFO and Fe_2O_3. Such a decrease is in good agreement with the values tabulated by Shannon [37] for high- and low-spin states. Additional Mössbauer spectroscopy and $R(P,T)$ are necessary in this case to clear an exact mechanism of the electronic transition.

V. CONCLUSIONS

In conclusion, a series of structural, electronic and magnetic transitions was observed in $GaFeO_3$ at the 0 – 70 GPa range. The structural instability of the partially low-coordination $Pc2_1n$ lattice results beyond 25 GPa in the more sturdier perovskite *Pbnm* structure, which undergoes at ~53 GPa the reversible isostructural transition corroborating with the *Mott* electronic transition to the uncorrelated HP Pv. Following decompression, the structurally related *R3c* structure becomes the stable one below 24 GPa, but at recompression it is replaced by the uncorrelated HP Pv at ~50 GPa.

Comparison of the present results with the *Fe*FeO_3 and *Ca*Fe_2O_4 data allows concluding that in all these ferric oxides the electronic transition to the uncorrelated state occurs at the same pressure, regardless of the preceding structures: *Pbnm, R3c* or $R\bar{3}c$, when the relative volume of the Fe-O_6 polyhedral V_{pol}/V_{0pol} reaches 0.84-0.85.

Acknowledgements: This research was supported in part by Israeli Science Foundation Grant #789/10, and the U.S. National Science Foundation and Department of Energy. We acknowledge the European Synchrotron Radiation Facility for provision of synchrotron radiation facilities beam line ID27. The Advanced Light Source is supported by the Director, Office of Science, Office of Basic Energy Sciences, of the U.S. Department of Energy under Contract No. DE-AC02-05CH11231.

Fig. 1. (Color online) The *Pc2₁n, Pbnm*, and the *R3c* crystal structures observed at various pressures in $GaFeO_3$. The red/orange (shinny/mat black), blue/pale blue (shinny/mat grey) and white spheres correspond to the Fe, Ga and O atoms at the different crystallographic sites, respectively. (Computer generated visualization based on T. C. Ozawa, S. J. Kang, J. Appl. Cryst. **37**, 679 (2004)).

Fig. 2. Mössbauer spectra in the 15 – 300 K range from which $T_N \approx 200$ K has been derived. This value is consistent with a stoichiometric composition and minimal disorder.

Fig. 3. (Color online) Typical examples of analyzed integrated patterns of XRD spectra collected for the three main crystallographic structures at various stages of compression/decompression at 13, 63 and 0.2 GPa at RT and the differences between the observed and calculated profiles. Marks show the calculated peak positions. The Δ symbols correspond to the Pt pressure-marker, ▲ - to FeO contamination (<5%).

Fig. 4. (Color online) Pressure evolution of the unit cells volume of $GaFeO_3$. The solid, dotted, dash-dotted, and dashed lines are theoretical fits for the *Pc2₁n*, LP perovskite, HP perovskite, and $LiNbO_3$ (LN)-type phases using the BM2 EOS. The variables obtained were: $K_0 = 230(4)$ GPa, $V_0 = 312.2(4)$ Å^3 for the *Pc2₁n* structure; $K_0 = 296(25)$ GPa, $V_0 = 291.7$ (2.4) Å^3 for the LP perovskite structure; $K_0 = 383(48)$ GPa, $V_0 = 274.6(4.4)$ Å^3 for the HP perovskite structure, and $K_0 = 223(9)$ GPa, $V_0 = 298.7(8)$ Å^3 for the LN-type at decompression and recompression. The volume was normalized to six unit formulas of $GaFeO_3$, i.e. Z = 8 for *Pc2₁n* phase, Z = 4 for *Pbnm* orthorhombic perovskite, and Z = 6 for $LiNbO_3$-type *R3c* phase. The inset shows the relative volume of the FeO_6 polyhedron for all phases as a function of pressure. Note a polyhedron volume drop at $V_{pol}/V_{0pol} \sim 0.85$. The solid and open symbols correspond to the compression and decompression cycles, respectively.

Fig. 5. Pressure dependence of the magnetic ordering temperature T_N. It reaches 300 K at ~ 33 GPa and in the 33 – 67 GPa pressure range $T_N > 300$ K. At 67 GPa it decreases to RT after which T_N precipitously reaches ~5 K at 77 GPa.

Fig. 6. (Color online) Mössbauer spectra recorded at 15 K for various pressures. The H_{hf} is typical of the Fe^{3+} oxides and reflects the magnetization at saturation ($T << T_N$) as a function of pressure. Up to 56 GPa this is the only spectral component. At 62 GPa a non-magnetic quadrupole-split component (dotted line) appears with relative abundance increasing with pressure. There is no apparent spectral change up to 98 GPa. The absence of magnetic components down to the lowest temperature of 5 K (85 GPa spectrum) strongly supports the onset of the MT characterized by the magnetic collapse due to the *d-d* correlation breakdown. The decompression spectrum does not show any sign of *sites distributions.*

Fig. 7. (Color online) The pressure dependence of the IS (●,○) and the relative abundance (■) of the nucleated metallic-nonmagnetic $GaFeO_3$. Their functional dependence upon $\Delta V/V_0$ (= $|V-V_0/V_0|$) reflects the proper variation of the molar volume shrinkage considering the fact that along the *P*-path various structures emerge with diverse bulk modulus values. As can be seen the IS decreases with pressure, namely the *s*-density at the nucleus ρ_s increases linearly with the fractional decrease of the molar volume. At 0.225 (*P*~62 GPa) an abrupt drop in the IS is observed, corresponding to an abrupt increase in the $\rho_s(\Delta V/V_0)$, signaling the sharp decrease of the <Fe-O> distances. At the same $\Delta V/V_0$ value one observes a drastic increase in the metallic nonmagnetic component reaching 100% at ~ 80 GPa.

Fig. 8. The variation of $R(P)$ with $\Delta V/V_0$ at RT. A sharp decrease in *R* is observed in the 0 – 0.08 $\Delta V/V_0$ range (0 – 20 GPa) taking place at the *Pc2₁n* phase. Following the onset of the perovskite phase the change in $R(P)$ is more gradual till $\Delta V/V_0 \sim 0.20$, where the electrons delocalization is triggered by *d-d* or *p-d* gap closure, reaching a metallic state at $P \sim 68$ GPa (see lower inset). The

$R(\Delta V/V_0)$ behavior in this range is very similar to that of $\rho_s(\Delta V/V_0)$ in the same pressure range (see Fig.7) in accordance with the *MH* theory.

REFERENCES

[1] W.M. Xu, O. Naaman, G. Kh. Rozenberg, M.P. Pasternak, and R.D. Taylor, Phys. Rev. B**64**, 094411 (2001), W. M. Xu, M. P. Pasternak, G.Kh. Rozenberg, and R. D. Taylor, Hyperfine Interactions 141/142 243 (2002),G. Kh. Rozenberg, M. P. Pasternak, W. M. Xu, L. S. Dubrovinsky, S. Carlson and R. D. Taylor. Europhys. Lett. **71**, 228 (2005)

[2] A. G. Gavriliuk, V. V. Struzhkin, I. S. Lyubutin, S. G. Ovschinnikov, M. Y. Hu and P. Chow Phys. Rev. **B77**, 155112 (2008) and references therein.

[3] M. P. Pasternak, G. Kh Rozenberg, G. Yu. Machavariani, O. Naaman, R. D. Taylor and R. Jeanloz, Phys. Rev. Lett. **82**, 4663 (1999)

[4] J. Staun Olsen, C. S. G. Cousins, L. Gerward, H. Jhans, and B. Sheldon, Phys. Scr. **43**, 327 (1991).

[5] G.Kh. Rozenberg, L.S. Dubrovinskii, M.P. Pasternak, O. Naaman, T. Le Bihan, R. Ahuja, Phys. Rev. B**65,** 064112 (2002).

[6] T. Arima, D. Higasiyama, Y. Kaneko, J.P. He, T. Goto, S.Miyasaka, T.Kimura, K. Oikawa, T. Kamiyama, R. Kumai and R. Tokura. Phys. Rev. B**70,** 064426 (2004), and references therein.

[7] K. Uk Kang, S. B. Kim, S. Y. An, S. W. Cheong, C. S. Kim., J. Mag. Mag. Mat., **304**, e769 (2006).

[8] E. Sterer, M.P. Pasternak, and R.D. Taylor, Rev. Sci. Instrum. **61** 1117 (1990).

[9] G.Yu. Machavariani, M.P. Pasternak, G.R. Hearne, and G.Kh. Rozenberg, Rev. Sci. Instrum. **69,** 1423 (1998).

[10] Mössbauer measurements at ambient pressure (Fig. 2) show large line widths compared to the typical line width associated with the lifetime of 3/2 spin state of ^{57}Fe. Previous authors [W. Kim, J. H. We, S. J. Kim, and C. S. Kim, J. App. Phys. **101**, 09M515 (2007)] calculated this Mössbauer spectrum using four Fe sites. In this research however the resolution level is not high enough in order to follow the evolution of all 4 sub spectra (and up to 6 near the phase transition) as a function of pressure, and so their decomposition was forfeited. Considering the limited resolution and the numerical error resulting from it their fit doesn't differ from ours, and our value of H_{hf} should be taken as an average.

[11] A.P. Hammersley, ESRF Internal Report, ESRF97HA02T, (1997).

[12] A.P. Hammersley, S.O. Svensson, M. Hanfland, A.N. Fitch, and D. Häusermann, High Pressure Research, **14**, 235 1996).

[13] A.C. Larson and R.B. Von Dreele, *General Structure Analysis System (GSAS)*, Los Alamos National Laboratory Report LAUR 86-748 (1994).

[14] B.H. Toby, *EXPGUI,* J. Appl. Cryst. **34**, 210 (2001).

[15] H.K. Mao, J. Xu, and P.M. Bell, J. Geophys. Res. **91** (1986) p. 4673.

[16] A.D. Chijioke, W.J. Nellis, A. Soldatov, and I.F. Silvera, J. Appl. Phys. **98**, 114905 (2005).

[17] Pressure at cryogenic temperature with our DAC's, increases slightly, by ~ 1 GPa with respect to RT. This is within the experimental error

[18] J.C. Jamieson, J.N. Fritz, and M.H. Manghnani, in High-Pressure Research in Geophysics, S. Akimoto and M. H. Manghnani, eds., Center for Academic Publishing, Tokyo, pp. 27-48, (1982).

[19] Y. Kaneko, T. Arima, J.P. He, R. Kumai, and Y. Tokura, J. Magn. Magn. Mater. **272**, 555 (2004)

[20] O. L. Anderson, *Equations of State of Solids for Geophysics and Ceramic Science*. Oxford, (1995)

[21] M. Marezio, J. P. Remeika and P. D. Dernier, Acta Cryst. B26, 2008 (1970). The extrapolated atomic positions are: Ga: (0.972,0.082,0.25), Fe: (0,0.5,0), O1: (0.163,0.416,0.25), O2: (0.674,0.321,0.092).

[22] The raison d'être for choosing $\Delta V/V_0$ (= $|V-V_0|/V_0$) instead of P as the variable are the changes in the bulk modulus taking place while crossing the various several phases along the 0 -80 GPa path. The $\Delta V/V_0(P)$ variable does away with this problem

[23] IS $\approx -\Delta R/R \times \rho_s(0)$ where $\Delta R/R$ is the relative change between the excited and ground-states of the ^{57}Fe nuclear radii.

[24] At a fixed pressure the resistivity data fairly accurately obey the relation of $lnR = lnR_0 + E/k_BT$, where k_B is Bolzmanns constant, E – electrical transport activation energy. At the 40 – 53 GPa range the value of E decreases more than twice: from 0.37 to 0.17 eV.

[25] Lowest accessible by our cryogenic system.

[26] The relative abundance of spectral component i is $A_i f_i \Big/ \sum_{j=1}^{n} A_j f_j$ where A is the derived value of the area of the absorption component, f is the the recoil-free fraction of the component, and n is the number of components. Here we assume as first approximation identical values of $f(\theta_D)$ for each component (θ_D – Debye temperature).

[27.] K. Leinenweber, Y. Wang, T. Yagi, H. Yusa, Am. Miner. **79**, 197(1994)) concluded that the high-pressure perovskites phases that transform to lithium niobates at low pressure all have tolerance factors (t) below ~0.84, whereas stable perovskite phases have tolerance factors above 0.84. In our case $t \approx 0.73$, therefore the transition to LN phase at the decompression is expected. (Look also H. Yusa, M. Akaogi, N. Sata, H. Kojitani, R. Yamamoto, Y. Ohishi, Phys. Chem. Minerals **33**, 217 (2006) and references therein.).

[28] H. Boysen, F. Altorfer, Acta Cryst. **B50**, 405 (1994).

The refined atomic positions are: Ga: (0,0,0.307), Fe: (0,0,0.0165), O: (-0.01,0.322,0.081)

[29] R. Ramirez, L. M. Falicov and J. C. Kimball, Phys. Rev. B**2,** 3383 (1970).

[30] Differences may also arise from the higher sensitivity of the synchrotron XRD method, where the higher signal/noise allows detection of new components at a level where its relative abundance is too small for Mössbauer spectroscopy.

[31] M. Merlini, M. Hanfland, M. Gemmi, S. Huotari, L. Simmonelli, and P. Strobel., Am. Miner. **95,** 200 (2010)

[32] H. D. Megaw, Acta Cryst. **A24**, 583 (1968).

[33] X. Wu, G. Steinle-Neumann, O. Narygina, C. McCammon, L. Dubrovinsky, High Pressure Research, **30,** 395 (2010).

[34] Y. Sato, and S. Akimoto, J Appl. Phys., **50**, 5285 (1979).

[35] L. W. Finger, and R. M. Hazen, J Appl. Phys., **51**, 5362 (1980).

[36] The crystallographic transition of the corundum phase into the Rh_2O_3-II structure by itself is accompanied by a volume decrease of ~4% (see R. D. Shannon and C. T. Prewitt, J. Solid State Chem. **2**, 134 (1970); N. Funamori and R. Jeanloz, Science **278**, 1109 (1997)). Therefore the part of the volume reduction associated with the electronic transition in Fe_2O_3 is ~6%.

[37] R.D. Shannon, Acta Cryst. **A32**, 751 (1976).

Table 1. The refined structural parameters of the $Pc2_1n$ and of the *Pbnm* perovskite (compression and decompression) phases at various pressures. Italic represents data from the decompress cycle.

P (GPa)	*a* (Å)	*b* (Å)	*c* (Å)
$Pc2_1n$ phase			
0.0001	8.7347(14)	9.3850(15)	5.0791(9)
3.6	8.649(11)	9.306(14)	5.072(9)
5.3	8.634(18)	9.27(2)	5.057(13)
7.1	8.640(26)	9.246(30)	5.05(2)
12.7	8.580(7)	9.210(6)	5.025(5)
13.5	8.54(1)	9.185(8)	5.041(6)
15.0	8.580(22)	9.14(3)	5.017(16)
15.7	8.554(12)	9.136(10)	5.013(7)
17.2	8.487(12)	9.137(10)	5.022(6)
18.0	8.503(12)	9.145(23)	5.008(14)
21.7	8.502(11)	9.038(10)	4.9970(45)
22.8	8.384(23)	9.10 0(24)	5.023(20)
25.7	8.417(15)	9.005(16)	4.974(20)
26.1	8.303(26)	9.034(30)	5.063(20)
29.3	8.240(18)	9.043(25)	5.052(16)
38.4	8.370(35)	8.80 0(18)	4.94(2)
42.1	8.387(24)	8.792(20)	4.933(23)
LP Perovskite phase			
25.7	4.948(4)	5.165(20)	7.000(18)
38.4	4.948(12)	5.077(20)	6.963(9)
42.1	4.946(10)	5.068(14)	6.947(10)
45.3	4.917(10)	5.066(13)	6.922(10)
50.6	4.926(10)	5.015(11)	6.884(8)
53.3	4.893(8)	5.035(7)	6.870(9)
53.0	4.904(13)	5.025(16)	6.902(10)
50.3	*4.942(17)*	*5.023(20)*	*6.897(8)*
40.3	*4.937(16)*	*5.080(17)*	*6.941(8)*
35.1	*4.971(6)*	*5.110(23)*	*6.955(7)*
24.3	*4.991(10)*	*5.142(18)*	*7.020(16)*
HP perovskite phase			
53.0	4.795(10)	4.950(12)	6.925(14)
56.1	4.796(10)	4.942(20)	6.897(23)
58.5	4.788(5)	4.939(6)	6.886(8)
61.2	4.782(10)	4.935(11)	6.882(12)
60.1	4.784(4)	4.922(13)	6.886(10)
63.6	4.7754(30)	4.924(20)	6.870(17)
63.5	4.775(3)	4.92(2)	6.874(20)
50.3	*4.793(6)*	*4.968(4)*	*6.937(7)*

Table 2. The refined structural parameters of the LN-type and HP perovskite (decompression and recompression) phases at various pressures. Italic represents data from the decompression cycle.

P (GPa)	*a* (Å)	*b* (Å)	*c* (Å)
LN phase			
24.3	*4.920(8)*	*4.920(8)*	*13.00(4)*
14.7	*4.968(2)*	*4.968(2)*	*13.188(10)*
0.2	*5.036(2)*	*5.036(2)*	*13.585(7)*
3.2	5.0235(14)	5.0235(14)	13.480(5)
5.5	5.0094(12)	5.0094(12)	13.436(5)
8.2	4.9977(13)	4.9977(13)	13.397(5)
12.2	4.9737(15)	4.9737(15)	13.314(6)
15.8	4.9570(14)	4.9570(14)	13.245(5)
19.1	4.9378(14)	4.9378(14)	13.179(5)
23.1	4.9172(15)	4.9172(15)	13.105(6)
27.9	4.8967(17)	4.8967(17)	13.023(6)
32.9	4.8765(18)	4.8765(18)	12.936(6)
38.3	4.8607(17)	4.8607(17)	12.867(6)
39.0	4.8550(17)	4.8550(17)	12.839(6)
42.4	4.849(2)	4.849(2)	12.790(7)
44.1	4.844(2)	4.844(2)	12.751(7)
46.2	4.8423(20)	4.8423(20)	12.714(8)
48.6	4.8390(27)	4.8390(27)	12.644(9)
50.8	4.824(5)	4.824(5)	12.672(10)
52.8	4.815(7)	4.815(7)	12.665(13)
HP perovskite phase			
50.8	4.794(10)	4.954(6)	6.937(10)
52.8	4.784(8)	4.950(4)	6.937(9)

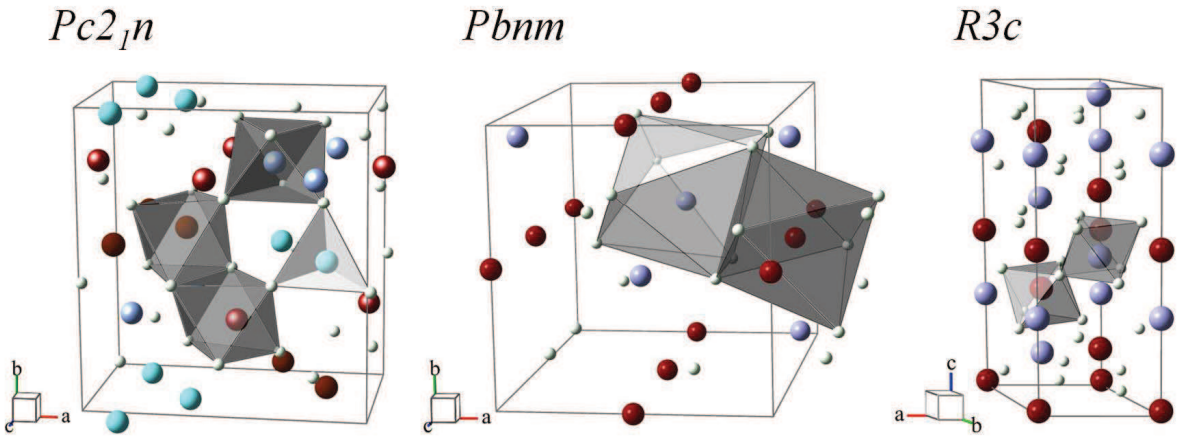

Figure 1 BF11615 05AUG2011

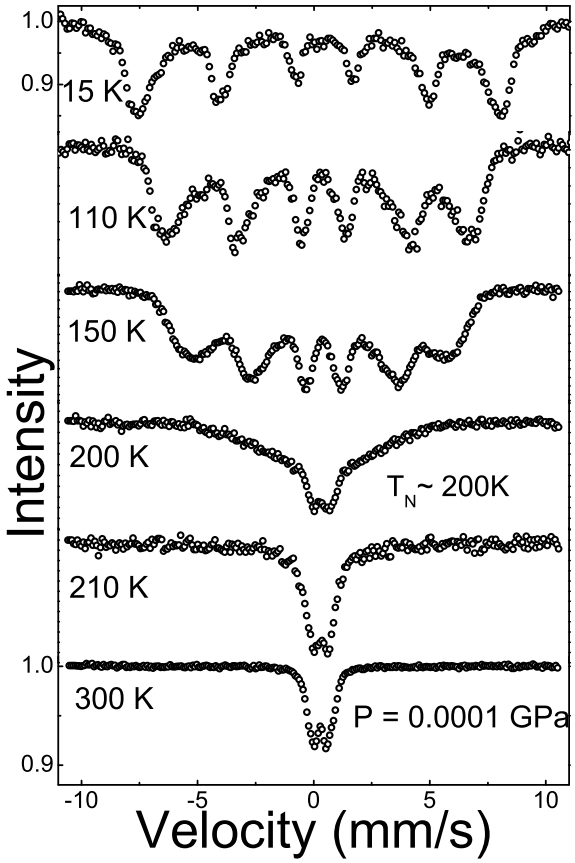

Figure 2 BF11615 05AUG2011

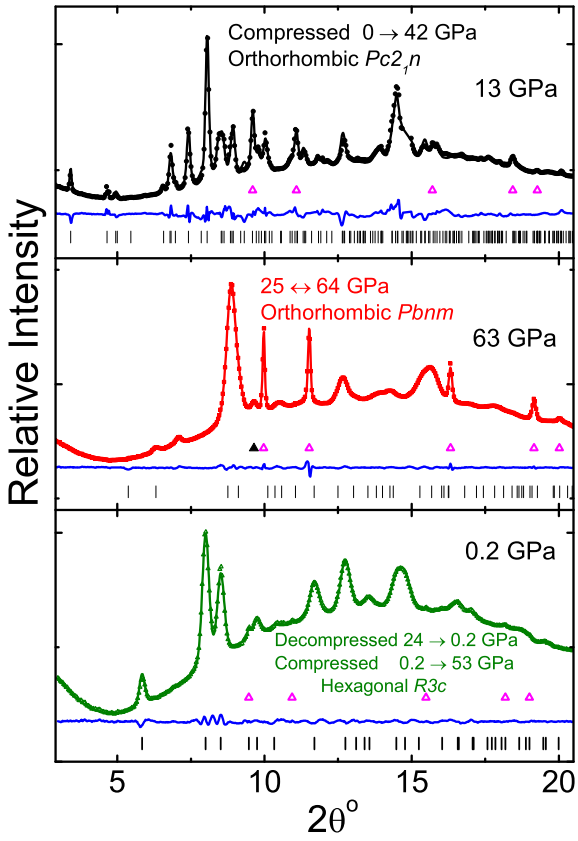

Figure 3 BF11615 05AUG2011

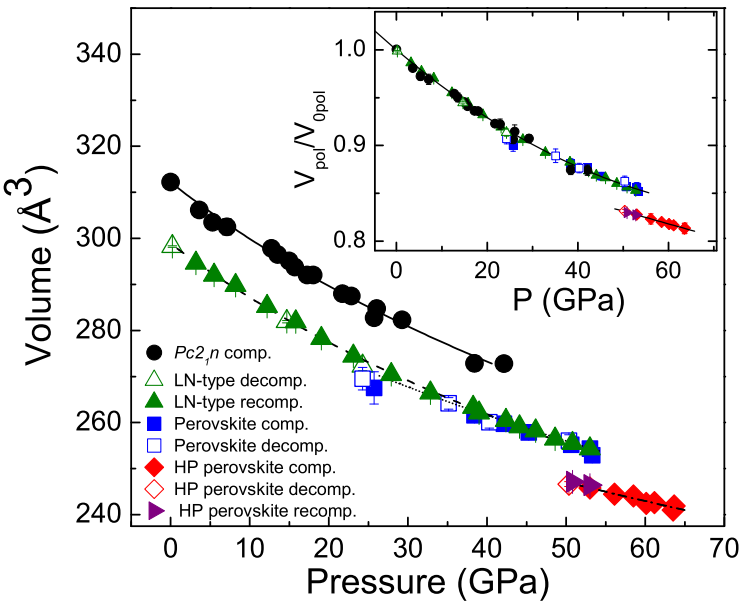

Figure 4 BF11615 05AUG2011

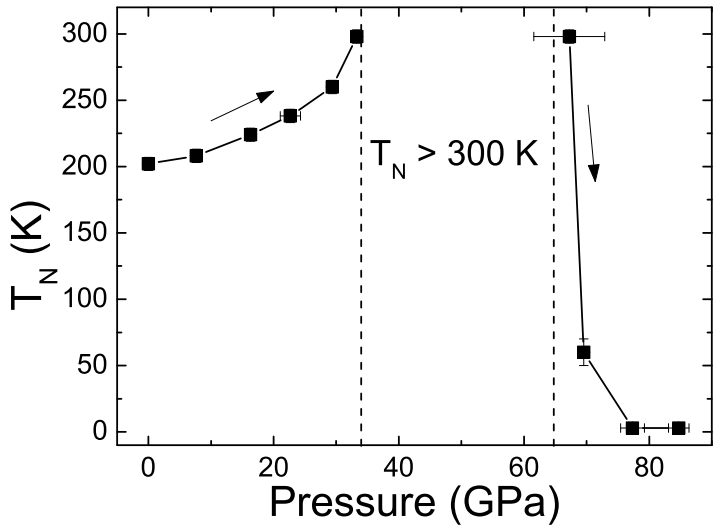

Figure 5 BF11615 05AUG2011

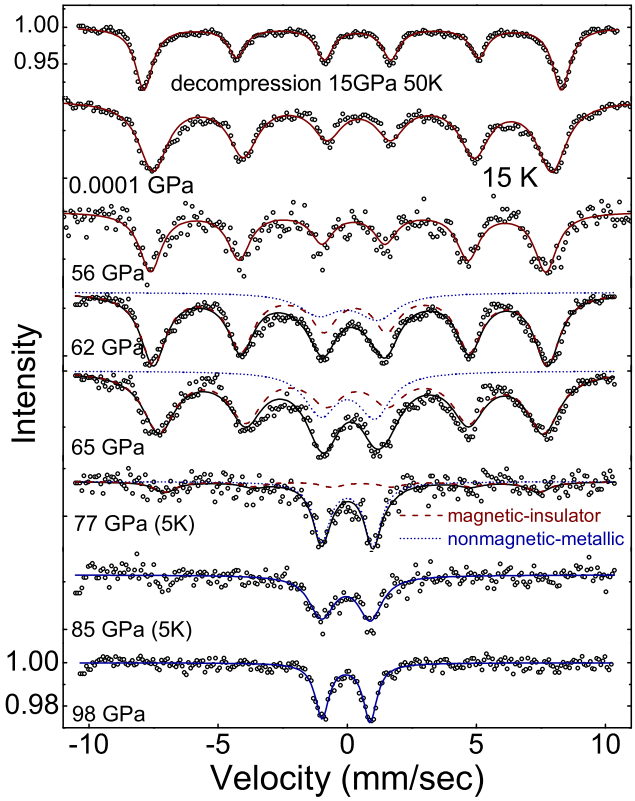

Figure 6 BF11615 05AUG2011

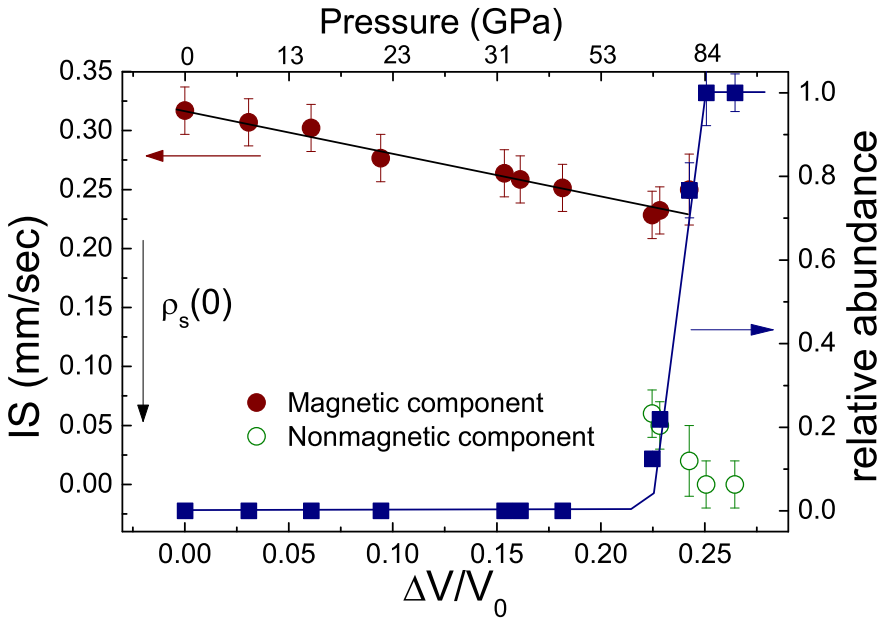

Figure 7 BF11615 05AUG2011

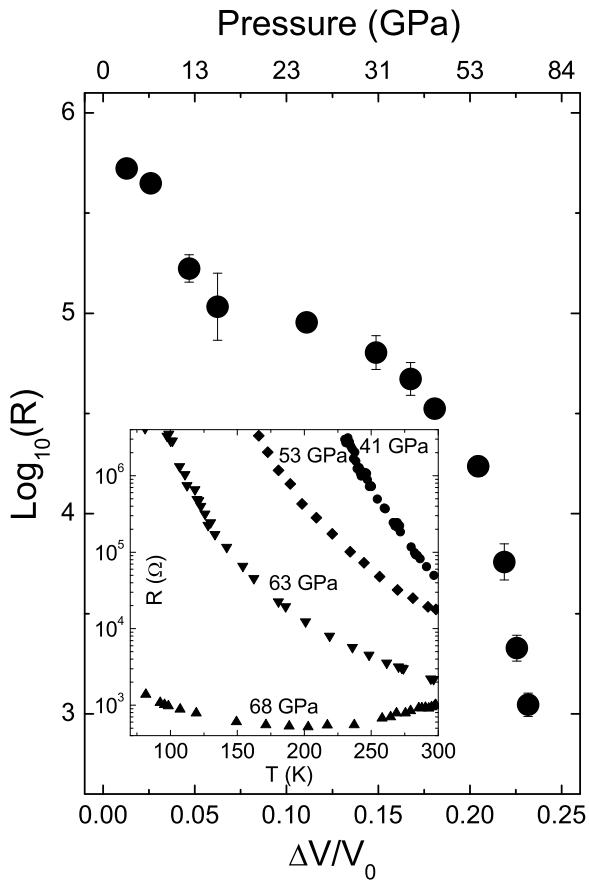

Figure 8 BF11615 05AUG2011